INSIGHT FROM THE STUDY OF FAST PYROLYSIS OF *ISOBERLINIA DOKA*-DERIVED SAWDUST FOR BIO-OIL PRODUCTION USING COMPUTATIONAL FLUID DYNAMICS APPROACH

Moritiwon, O. J.[1]; Afolabi, E. A.[2*]; Garba, M. U.[3]; & Aboje, A. A.[4]

[1,2,3,4] Department of Chemical Engineering, Federal University of Technology, P.M.B 65, Gidan Kwano-Minna, Niger State, Nigeria . Morale92@yahoo.com; *elizamos2001@yahoo.com; umar.garba@futminna.edu.ng; alen248@futminna.edu.ng)

ABSTRACT

The conversion of biomass to bio-oil is now receiving more attention as it provides an alternative source of energy and raw materials for many industries. However, the ability to control the process of maximizing its yield and quality is at its preliminary stage. Hence, investigating bio-oil conversion with ANSYS FLUENT, a commercial Computational Fluid Dynamics (CFD) code was necessary. Eulerian multiphase model coupled with the kinetic theory of granular flow was used to resolve the flow-dependent process occurring in the reactor which had been modified to mimic a fluidised behaviour in the bed zone for experiments and now, simulations. Hydrodynamics as well as specie exchange-enabled simulations were carried out with temperature varied between 400-500 ^{0}C. Particle size category 0.5 - 1 mm was adopted for simulation instead of <0.5 range based on experimental findings. Hydrodynamic behaviours of gas-specie flow shows that the process is temperature, pressure and velocity dependent. Also, pressure drop was observed over the height of reactor which became marginal within the reaction zone. Predicted bio-oil yield validated experimental data but indicated possibility of better bio-oil recovery if process parameters are strictly controllable experimentally.

Keywords: Bio-oil; Isoberlinia doka; Fluid dynamics; Yield; Temperature

INTRODUCTION

Fast Pyrolysis is a viable technology for bio-oil recovery from lignocellulosic biomass because of its value as a renewable fuel for transportation and as a precursor for specialty chemical manufacture (Adkins *et al*., 2017; Yildiz *et al*., 2016; Butler *et al*., 2011). Although a promising technology yet, it is at a laboratory stage and faced with several challenges that can be resolved over time by continuous research. Experimental means of investigation are common and are highly reported but are limited by the extent to which researching can be done. Some of these limitations are risks of explosion and human harm of some processes as well as organic volatile interference with instrumentation. Visual windows are also obscure, inaccurate and unapproachable due to fervent heat. In contrast, the virtual laboratory offered by the CFD simulation approach can be fruitful if remediated with little experimentation to validate its findings that are predictive in nature (Jin *et al.,* 2023; Wang and Chen, 2012). CFD entails the swapping of partial differential equations (PDEs) systems for algebraic equations which can be solved using high-end computers thus, performing an experiment without a physical laboratory (Versteeg and Malalasekara, 2007). These PDEs represents conservation laws for mass, momentum, and energy that govern the pyrolysis process. CFD may not replace experiments completely in some cases but it does significantly reduce the overall cost as well as the amount of experimentation required.

Simplified fluid dynamics descriptions are commonly used as a basis for engineering models. For solid-gas flow models, more detailed descriptions are required and can be obtained from the solutions of Navier-Stokes equations (Raval, 2008). When the number

of particles in the gas phase is too large (typically > 10^6), Newtonian equations are to be paired with Navier-Stokes to arrive at an average to save cost computationally (Ramisetty, 2010). Anca-couce, (2016) explained reaction kinetics and multi-scale modelling as it concerns lignocellulosic biomass pyrolysis mentioning two main approaches to cases involving solid-gas flows. One of the approaches require coupling of the fluid phase to the Langragian phase while the other is the Two-Fluid (TF) model which treats both phases as fluids. The former was adopted by Ku *et al.* (2015) who modelled a biomass gasification process tracking each particle was considered individually using the Eulerian-Langrangian model. These particles were found to exhibit multiple physical and thermo-chemical properties. Despite the success in tracking, central processing unit (CPU) overload was observed due to strenuous particle collision monitored as the number of particles increased. In like manner, Gerber and Oevermann (2014) conducted a parametric study for a Euler-Langragian model applicable to wood gasification with emphasis on primary and secondary pyrolysis in a fluidized bed but, with a bi-disperse mixture of 12,000 charcoal particles. Multiple particle-particle collisions were reported from their findings indicating that this model is an overlaod for this problem type except for particle dependent scenarios. The TF models (standalone or in attachment with granular flow theory) are adjudged to be better trimmed for simulation involving gas-solid flows.

The TF model options include the mixture, volume of fluid (VOF) and Eulerian models with latter outperforming others in a non-stationary particle situation. The Eulerian-Eulerian multiphase model is characterised by lesser computational requirements and is sufficient for low particle laden flows compared to the Eulerian-Lagrangian model and the direct numerical simulation approach (DNS). Liu *et al*. (2017) utilised this method to model particle shrinkage in a fast pyrolysis process occurring in a fluidised bed. An evolution of particle sizes with density variations were obtained from their experiments and can be attributed to continuous devolatilisation.

The Eulerian-Eulerian model handles this case type in a peculiar manner. It assumes that both the gas and solids are in a continuous phase thus, describing the solid-gas interactions with both the drag and averaged collision models (Jin *et al*; 2023; Almohammed *et al*., 2014). Although, this model is computationally attractive, the presence of flow instabilities shows its limitations. This creates a distraction to the determination of coefficients and correlations that describes the drag or particle collisions from experimental data. Attaching the granular model can remediate the particle handling limitation of the Eulerian model if solid load is low. Eri *et al.* (2018) carried out a biomass steam gasification simulation using detailed kinetic schemes based on the TF model and kinetic theory of granular flow. Their findings showed that the proposed model gave satisfactory particle accounting and identified that the inlet gas temperatures is a major influence on the process. Also, considering that the condensable bio-oil and non-condensable gases (NCG) co-exist as gas-specie in the reactor prior to condensation, the Eulerian part of the model handles the gas-specie containing the desired product. Furthermore, particle to particle heat transfer can be neglected in this model. Such was reported by Shu *et al.* (2015) who evaluated multifluid model for heat transfer behaviour in binary gas-solid flow. It was found that in downer reactors, the effect of particle-particle heat transfer is negligible compared to the effect of gas-solid particle heat transfer. Therefore, this paper details fast pyrolysis using *Isoberlinia doka*-derived sawdust to investigate a modified fixed bed computationally. Experimentation was built upon with computers to synthesize bio-oil for yield. To achieve this, the flow of the gaseous phase, particle phase, and extensive equations based on physical and chemical

theory obtainable in the reactor was applied. In addition, experimental data were used to validate simulation results.

COMPUTATIONAL METHODOLOGY

Model and Mathematical Approach

A block flow diagram showing the stagewise approach used in simulating the pyrolysis process in the ANSYS Fluent environment is shown in Fig. 1. ANSYS Design Modeler was used to construct a 3-dimentional (3-D) geometry of the modified fixed bed reactor from the experimental set up of Moritiwon *et al.* (2021) as shown in Figs. 2-3. Eulerian-granular model was used to describe the carrier gas and biomass in a multiphase while patching the reactor initially at 40 % to indicate the biomass bed limit. The Eulerian – granular model was chosen because of the fluid phase that is treated as a continuum by solving the Navier-Stokes equations, while the particle-particle interactions can be neglected. Therefore, as observed by Runhui *et al.,* 2023 and Ruming *et al.,* 2023 the Eulerian-granular model captured the flow behaviour of the solid phase within the multiphase flow accurately.

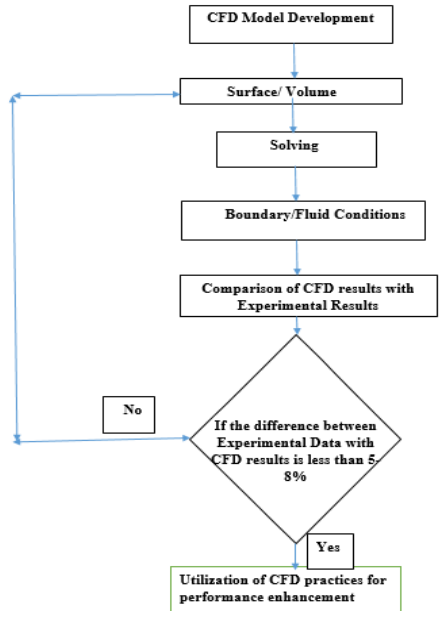

Fig. 1: Overview of CFD methodology

In transient calculations, governing equations were solved using FLUENT version 16.0. Formulation for the time dependent solution was first order implicit while gradient was spatially discretized based on the least squares cell approach.

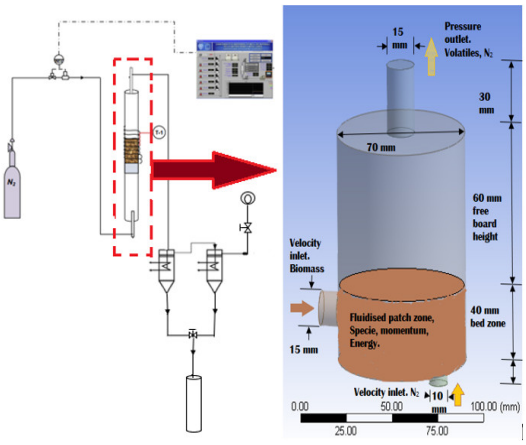

Fig 2a and b. Schematics from Moritiwon *et al.* (2021) (left) and Computational domain of the present study (right)

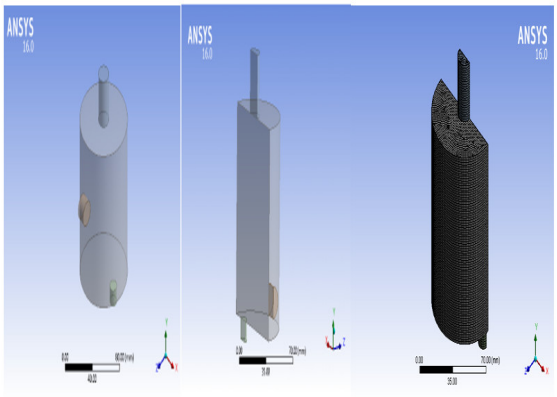

Fig 3. Full reactor geometry(left). Geometry with symmetry on the XY plane (Middle). Meshed geometry (Right).

All other variables were based on the first order upwind scheme. phase coupled SIMPLE algorithm was used for the pressure-velocity coupling while convergence criterion for energy transport equation was set to 10^{-6}. Other equations were set to converge at 10^{-3}. Under-relaxation factors were set to 0.5 for pressure, 0.7 for momentum, 0.8 for turbulent species, 0.5 for volume fraction, 0.2 for granular temperature, and default for other quantities.

A time step of 1×10^{-10} s was found to be suitable for the grid size of the domain (ANSYS Fluent, 2021c). A multicore processor AMD® APU® with 12 GB of RAM completed the calculations in a total computational time of 12 weeks (4 weeks per case) for a real-time of 10.75s.

Meshing

Meshing was carried out using ANSYS ICEM obtaining mesh properties at element sizes ranging from 1–1.5 mm as shown in Table 1. Multizone method was used to generate meshes which were tested for grid convergence using K-epsilon-2-equation model and enhanced wall treatment to select optimum mesh (ANSYS Fluent, 2021a).

Table 1. Mesh properties at different mesh sizes

Mesh size (mm)	Orthogonal quality min(10^{-1})	Orthogonal skew max (10^{-1})	Maximum aspect ratio
1.50	7.04	2.96	6.36
1.25	6.99	3.01	3.88
1.15	8.69	1.31	3.03
1.00	7.95	2.05	3.59
Adapted	8.69	1.31	3.03

Table 2. Grid test and adaptation of geometry

Code	Mesh size, mm	Cell	Face	Node
A	1.50	63402	195842	069242
B	1.25	106244	326688	114443
C	1.15	137808	422874	147522
D	1.00	206334	631376	219009
E	Adapted	140510	445052	151509

Optimum mesh selected was then, adapted at 10 % gradient refine threshold to allocate more cells to result dependent regions of the mesh. Final mesh contained 4 cell zones and 29 face zones with nodes as shown in Table 2. Adaptation of optimum mesh resulted in the increase of cell volume by 1.96 %, faces by 0.034 % and node count by 2.68 %. This implies that more cell, node and faces were successfully placed in pressure dependent regions for accurate result.

Boundary Conditions

The outlet the reaction zone which is the topmost part of the reactor was quenched using reflux condenser experimentally at the temperature of 16 ^{0}C. Boundary conditions at the inlet, wall and outlet as adopted from Moritiwon *et al.* (2021) are presented by Equations 1-8.

BC at gas inlet $at\ L = 0,\ 0 \le r \le D$:

BC1-3 $\vec{v} = v_{gin} = 4$ m/s, (1)

BC1: $\varnothing = \varnothing_g = 160\ ^0$C/min, $T_{gin} = T_{g1} = 400\ ^0$C, (2)

BC2: $\varnothing = \varnothing_g = 160\ ^0$C/min, $T_{gin} = T_{g2} = 450\ ^0$C, (3)

BC3: $\varnothing = \varnothing_g = 160\ ^0$C/min, $T_{gin} = T_{g3} = 500\ ^0$C. (4)

BC at biomass inlet $at\ L = 0.003$ m, $0 \le r \le D$: (5)

BC1-3 $\vec{v} = v_{sin} = 0.003838$ m/s,

$M_s = M_{sl} = 0.03$ Kg, $T_s = T_{sin} = 25\ ^0$C, (6)

BC of the wall at every side of the geometry BCs:

BC1-3 $\vec{v} = v_{wall} = 0$ (7)

BC at the outlet:

BC1-3 $P_{out} = P_{atm} = 101325$ Pa (8)

Material Properties

Table 3. Flow and thermodynamic properties of nitrogen phase.

Property	Value(s)
Density	Incompressible fluid kg/m^3
Cp (Specific Heat)	(300-1000: 979.043, 0.418 - 0.002936e^{-6}, -1.157e^{-09}) J/k
Thermal Conductivity	0.0261 W/m-K
Viscosity	0.0000134 kg/m-s
Molecular Weight	18.015 kg/kgmol
Standard State Enthalpy	-2.418e^{08} J/kgmol
Reference Temperature	298.15 K

Table 4. Granular and thermodynamic properties of biomass phase.

Property	Units	Value(s)
Density	kg/m^3	700
Cp (Specific Heat)	J/Kg-K	2310
Thermal Conductivity	W/m-K	0.173
Molecular Weight Standard	kg/kgmol	100
State Enthalpy	J/kgmol	0
Reference Temperature	K	298.15
Diameter	m	0.0005
Vaporization temperature	K	400
Volatile fraction	%	80
Binary diffusion	m^2 /s	0.00004
Particle emissivity	-	0.9
Swelling coefficient	-	1
Burnout heat of reaction	J/kgmol	32789000
Devolatilization model	S^{-1}	20

Tables 3, 4 and 5 shows pre-defined material properties of nitrogen gas, wood-dust and correlations of viscosity for granular phase respectively. Subsequently, they were grouped into the fluid and the granular phases in the FLUENT setup (Jin and Xiaoke, 2023; Runhui *et al;* 2023). Phase property of mixtures like specific heat capacities (Cp) was calculated based on mixing law for both phases. For density (ρ), incompressible fluid model was used for the fluid phase while volume weighted-average mass weighted-average was adopted for the granular phase.

Table 5. Correlations for the viscosities of the solid phase

Viscosity term	Equation
Bulk viscosity (Equation 9) Lin *et al*. (2017)	$\lambda_s = \frac{4}{3}\alpha_s\rho_s d_s g_0(1 + \mathfrak{e}_s)\left(\frac{\Theta_s}{\pi}\right)^{1/2}$
Kinetic Viscosity (Equation 10) Sambal *et al*. (1993)	$\mu kinetic = \frac{\alpha_s\rho_s d_s(\mathfrak{e}_s\pi)^{\frac{1}{2}}}{6(3-\mathfrak{e}_s)}(+\frac{2}{5}(1 + \mathfrak{e}_s)(3-\mathfrak{e}_s)g_0\alpha_s)$
Collisional viscosity (Equation 11) Sambal *et al*. (1993)	$\mu_{coll} = \frac{4}{5}\alpha_s\rho_s d_s g_0(+\mathfrak{e}_s)\left(\frac{\Theta_s}{\pi}\right)^{1/2}\alpha_s$
Frictional viscosity (Equation 12) Johnson *et al*, (1990)	$\mu fric = \frac{\rho_s sin\Phi}{2(I_2 D)^{\frac{1}{2}}}$

Governing Equations

Equations 13 – 20 represent momentum, energy, chemical species, mass source term, turbulence intensity and laminar finite rate reaction as implemented in FLUENT.

Momentum

$$\frac{\partial\rho}{\partial t}(\alpha_g\rho_g\vec{v}_g) + \nabla\cdot(\alpha_g\rho_g\vec{v}_g\vec{v}_g) = -\alpha_g\nabla P + \nabla\tau_{\bar{\bar{g}}} - \beta(v_g - v_s) + \alpha_g\rho_g\vec{g}cos\theta + \dot{m}_{gs}\vec{v}_{gs} + \vec{R}_{sg} \quad (13)$$

$$\frac{\partial\rho}{\partial t}(\alpha_s\rho_s\vec{v}_s) + \nabla\cdot(\alpha_s\rho_s\vec{v}_s)$$

$$= -\alpha_s \nabla P_s + \nabla \tau_{\bar{\bar{s}}} - \beta(v_g - v_s) + \alpha_s \rho_s \vec{g} cos\theta + \dot{m}_{sg} \vec{v}_{sg} + \vec{R}_{gs} \quad (14)$$

Energy

$$\frac{\partial \rho(\alpha_g \rho_g h_g)}{\partial t} + \nabla \cdot \left(\alpha_g \rho_g \vec{v}_g h_g\right) = \alpha_g \frac{\partial \rho_g}{\partial t} + \tau_{\bar{\bar{g}}} : \nabla \vec{v}_g - \vec{q}_s + S_g + a_{gs} h_{c,gs} \left(T_g - T_s\right) + (\dot{m}_{gs} h_{gs} - \dot{m}_{sg} h_{sg}) \quad (15)$$

$$\frac{\partial \rho(\alpha_s \rho_s h_s)}{\partial t} + \nabla \cdot (\alpha_s \rho_s \vec{v}_s h_s) = \alpha_s \frac{\partial \rho_s}{\partial t} + \tau_{\bar{\bar{s}}} : \nabla \vec{v}_s - \vec{q}_s + S_g + a_{sg} h_{c,sg} A_i \left(T_s - T_g\right) + (\dot{m}_{sg} h_{sg} - \dot{m}_{gs} h_{gs}) \quad (16)$$

Chemical species

$$\frac{\partial \rho Y_i}{\partial t} + \nabla \cdot (\rho \bar{u} Y_i) = -\nabla \cdot \hat{J}_i + R_i + \dot{\omega}_i \quad (17)$$

Mass source term $S_m = \frac{\dot{m}_w Y_v}{Y_b}$ (18)

Turbulence intensity

$I = 0.16(Re_{Dh})^{-1/8} \times 100\%$ $(D_h = D)$, (19)

Laminar finite rate reaction

$$k_{f,r} = A_r \, T^{\beta} \left(e^{(-E)/RT}\right) \quad (20)$$

where $k_{f,r}$, A_r and T_β are the forward rate constant for the reaction, pre-exponential factor and temperature exponent. Equation 20 represents the forward only reaction. For this simulation, A_r is given as 4.12 x 10^6 S^{-1} while activation energy E is given as 112 KJ/mol (Almohammed *et al.,* 2014). Particle surface reaction was implemented using Equation 21.

Surface reaction $R = R_c(c_g - \frac{R}{D_0})^N$ (21)

Where C_g connotes reacting gas species concentration in the bulk and D_0 signify the bulk diffusion coefficient. Rc is the chemical reaction rate coefficient while C_s gives the mean reacting gas species concentration at the surface. Also, N stands for the apparent reaction order. Stoichiometric coefficients and one step global rate reaction for lignocellulosic biomass as obtained by Bashir (2017) was adopted as given in Equation 22:

$$Biomass \rightarrow \alpha_1 Char + \alpha_2 Oil + \alpha_3 Gas + \alpha_4 H_2O \quad (22)$$

$\alpha_1 - \alpha_4$ is given as 0.138, 0.805, 0.064 and 0.15 respectively. This represents the stoichiometric coefficient for char, oil, gas and water vapour (ANSYS Fluent, 2021 b and c).

RESULTS AND DISCUSSION

Reactor Hydrodynamic Behaviour

Fig. 4a shows the velocity magnitude as a result of the inlet gas flow. The mixing of solid particles is promoted by the solid motion around the rising bubble driven by the inlet velocity of the gas flow (Dinh *et al.*, 2017). Static or stagnation temperature of a moving gas is the temperature value measured at every point for every change in positioning for the gas flow (Eri *et al.* 2018, ANSYS Fluent, 2021b). It can be seen in Fig. 4b that temperature distribution is even and fixed at 313 K across the reactor. This implies that there is an equal amount of heat energy supplied to every point travelled by the carrier gas. Velocity component in the radial direction indicates the location of a particle away from or towards a reference point in a geometry (Bashir, 2017; ANSYS Fluent, 2021b). Fig 5a shows that most particles can be traced easily except for the ones found at the reactor side opposite to the gas inlet which may require dedicated particle tracking. Another component of velocity measured is tangential velocity usually in effect along the edge of a circle measured at any arbitrary instant (Gonzalez-Quiroga, 2017; ANSYS Fluent, 2021b). Since all zones are cylindrical in shape, every arbitrary point from the inlet to the outlet represent the circumference of a circle. Hence, gas can take a circular shape in a swirl leaving low velocity points at the centre as shown in Fig. 4b. Static pressure provides information about regions susceptible to low and high-pressure in the reactor (Gonzalez-Quiroga, 2017). A high-pressure distribution of between 4.52 and 5.12×10^3 kPa can be seen in the reaction zone which drops at the top of the reactor as shown in Fig. 6. This

Moritiwon, O. J.[1]; Afolabi, E. A.[2*]; Garba, M. U.[3] ; & Aboje, A. A.[4]

implies that the reaction zone is sufficiently pressurized to expel products once they form.

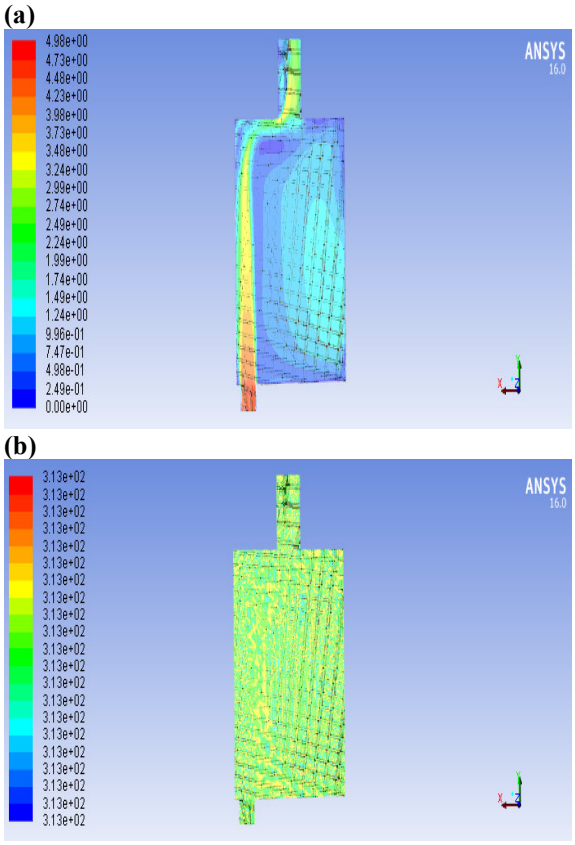

Fig 4: Contours showing (a) Velocity magnitude (b) Static temperature

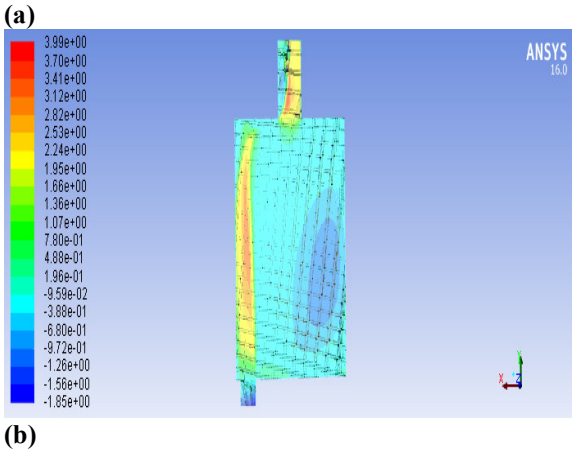

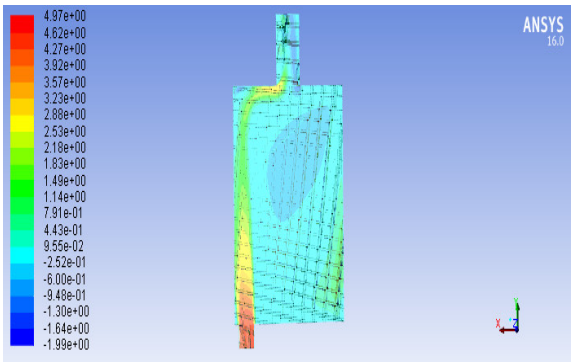

Fig 5. Contours showing (a) Radial velocity (b) Tangential velocity

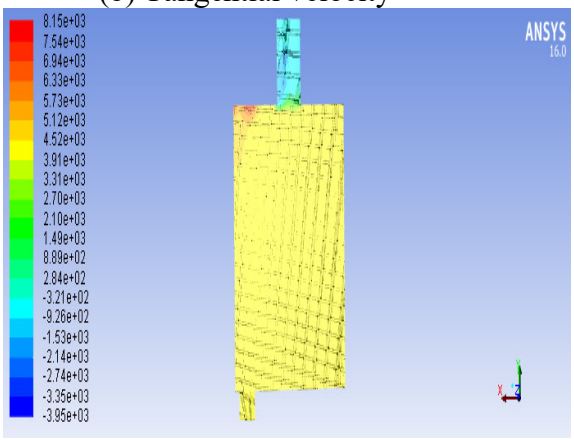

Fig 6. Contour showing Static pressure for adapted 1.15 mm mesh size

Pressure Drop

Fig. 7 shows pressure drop of volatile-gas specie mixture over reactor height. Gas flow is in the vertical direction against gravity (-9.81 m/s). Likewise, moving bed of biomass particles obstructs upward gas flow. It can be observed from the curve that there exist three pressure regimes within the reactor, each describing the various reactor zones.

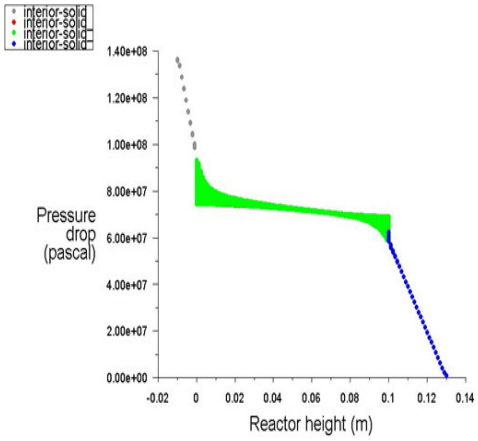

Fig 7. Pressure drop under Syamlal o' brien drag and Lengendre magnaudet lift effect (V_{0g}= 4 m/s, dp = 0.5-1 mm, biomasvolume fraction = 0.4)

The gas inlet zone which span from -0.01 to 0 m is characterised by a high but decreasing pressure attributed to the high velocity gas injection. The reaction zone extended from 0 to 0.1 m and is characterised by a moderately high but marginally constant pressure which is a result of the momentum breaking effect of solid particles. Also, the reactor design for sudden increase in diameter at the zonal interface and the effect of negative gravity contributed to such behaviour. The outlet zone marked at 0.1 to 0.13 m showed a decrease in pressure which can be attributed to the fairly constant pressure of the preceeding zone, negative gravity and the effect of distance already travelled by gas-specie. Sudden decrease in diameter at the interface zonal interface and the continous fluidisation of the system ensures overflow at the outlet.

Effect of Temperature on Bio-Oil Yield

Wood-dust experiment and simulation may be compared if Arrhenius equation is adopted to govern reactions in the latter (Yu *et al*. 2015). Fig. 8 shows the effect of temperature on bio-oil yield while comparing experimental with predicted results. It can be observed that predicted bio-oil yield increased as temperature increased following the experimental trend. It represented a 4.14 % increase for a 50 ^{0}C rise in temperature and a 11.31 % increase at 500 ^{0}C. These validate experimental records of 5.25 and 8.89 % increase at corresponding temperatures points.

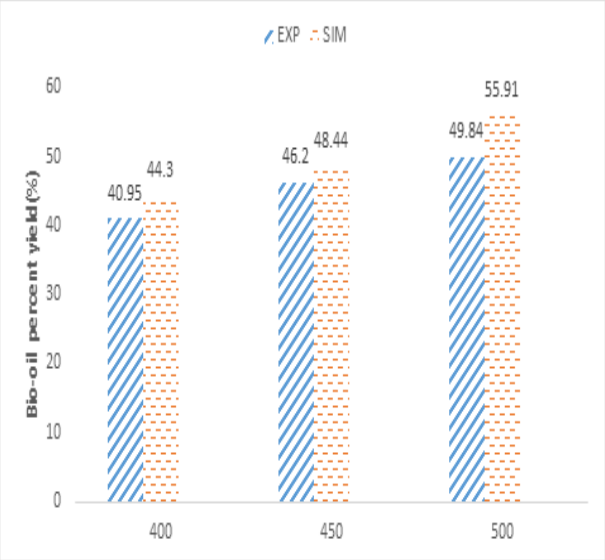

Fig 8. Experimental and predicted effect of temperature on bio-oil yield (0.5-1 mm particle size range, 30 minutes)

Validation of Predicted Pyrolysis Products

Fig. 9 shows predicted biochar, bio-oil and gas yield validated by experiments while Fig. 10 compares same with the results of Ding *et al*. (2012) who investigated fast pyrolysis of switch grass at 400 ^{0}C with the aid of an experimental circulating fluidized downer reactor and Punsuwan and Tangsathitkulchai (2014), who studied product characteristics in an experimental three zone free fall reactor at 520 ^{0}C. It can be seen that experimental data followed in the same trend observed with the results of simulation as displayed by Fig. 8. However, predicted biochar yield was higher by 3.68 % at 400 ^{0}C but decreased by 0.717 and 2.4 % at 450 and 500 ^{0}C respectively compared to experimental data. Also, predicted bio-oil yield increased by 3.35, 2.24 and 6.07 % while NCG decreased by 7.03, 1.52 and 3.67 % at these temperatures. This implies that higher bio-oil and total product yield obtained by simulation is a reflection of a better control over process variables which is a limitation to experimentation. Furthermore, Ding *et al*. (2014) and Punsuwan and Tangsathitkulchai (2014) findings can serve as upper and lower band for comparison to predicted results

despite that both literatures investigated a set up with a superior configurations and different feedstocks.

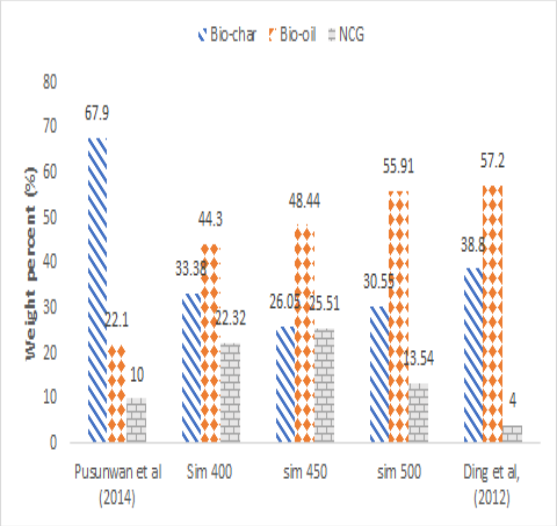

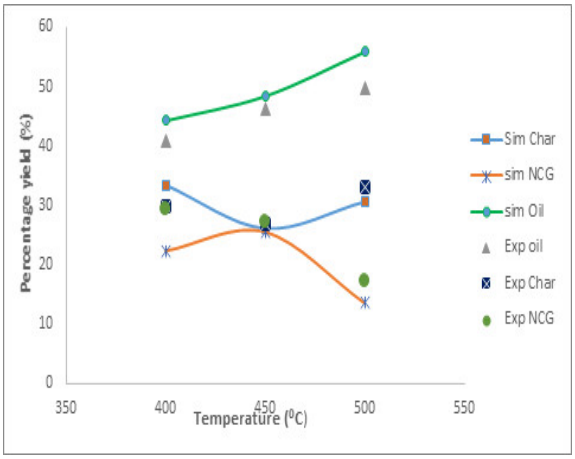

Fig.9. Validation of experimental product distribution with predictions (0.5-1 mm particle size range, 30 minutes)

Fig 10. Validation of Simulation results with experiment Data of Ding *et al.* (2014) and Punsuwan and Tangsathitkulchai (2014).

CONCLUSION

From the simulation carried out, it can be concluded that the reactor hydrodynamic properties which include temperature, pressure and velocity are factors on which the process is dependent. It can also be said that pressure drop within the reactor is associated with sudden change in diameter of reactor zone, solid drag in the reaction zone as well as the reactor height. In addition, although experimental bio-oil yield agrees with CFD prediction in a trend, improvement in experimentation can be made by tuning process parameters. Conclusively, validated model can be adopted for further investigations that are too difficult or/and dangerous to determine experimentally.

ACKNOWLEDGMENT

This work was supported by Petroleum Technology Development Fund in the framework of the local study scholarship (PTDF/ED/LSS/MSC/OMJ/394/17).

REFERENCES

Adkins, B. D.; Kapur, N., Dudley, T.; Webb, S. and Blaser P. (2017). Experimental validation of hy-drodynamic models for catalytic fast pyrolysis, *Powder Technology*, 316, 725–739. *http://dx.doi.org/10.1016/j.powtec.2016.11.060*

Almohammed, N.; Alobaid, F.; Breuer, M. and Epple, B. (2014). A comparative study on the influence of the gas flow rate on the hydrodynamics of a gas–solid spouted fluidized bed using Euler–Euler and Euler–Lagrange/DEM models, Powder Technology, 264, 343-364. *http://dx.doi.org/10.1016/j.powtec.2014.05.024*

Anca-couce, A. (2016). Reaction mechanisms and multi-scale modelling of lignocellulosic biomass pyrolysis, *Progress in Energy and Combustion Science*, 53, 41–79. *http://dx.doi.org/10.1016/j.pecs.2015.10.002*

ANSYS Fluent, (2021a). *ANSYS Fluent R 1 meshing user's guide,* ANSYS. Inc, 154-160.

ANSYS Fluent, (2021b). *ANSYS Fluent R 1 theory guide,* ANSYS. Inc, 596-600.

ANSYS Fluent, (2021c). *ANSYS Fluent R 1 users guide,* ANSYS. Inc, 74-90.

Bashir, M. A. (2017). *A novel approach for integrating concentrated solar energy with biom-ass thermochemical conversion processes*, Ph.D. thesis, Aston University. *http://publication. aston.ac.uk/id/eprint/30868/*

Butler, E.; Devlin, G.; Meier, D. and McDonnell, K. (2011). A review of recent laboratory research and commercial developments in fast pyrolysis and upgrading, *Renewable and Sustainable Energy Reviews*, 15 (8), 4171–4186. *http://dx.doi.org/ 10.1016/j/rser.2011.07.035*

Ding, T.; Li, S.; Xie, J.; Song, W.; Yao, J. and Lin, W. (2012). Rapid pyrolysis of wheat straw in a bench-scale circulating fluidized-bed downer reactor, *Chemical Engineering Technology*, 35, 2170–2176. *http:// dx.doi.org/10.1002/ceat.201200140*

Dinh, C. B.; Liao, C. C. and Hsiau, S. S. (2017). Numerical study of hydrodynamics with surface heat transfer in a bubbling fluidized-bed reactor applied to fast pyrolysis of rice husk. *Advanced Powder Technology*, 28, 419–429. *http://dx.doi.org/ 10.1016/j.apt.2016.10.013*

Eri, Q.; Peng, J. and Zhao, X. (2018). CFD simulation of biomass steam gasification in a fluidized bed based on a multi-composition multi-step kinetic model, *Applied Thermal Engineering*, 129, 1358-1368. *https://doi.org/10.1016/j.applthermal eng.2017.10.122*

Gerber, S. and Oevermann, M. (2014). A two-dimensional Euler-Langragian model of wood gasification in a charcoal bed-part 1: model description and base scenario, *Fuel*, 115, 385-400 *Http://doi.org/10.1016/j.fuel.2013.06. 049*

Gonzalez-Quiroga, A.; Reyniers, A. P.; Kulkarni, S. R.; Torregrosa, M. M.; Perreault, P.; He- ynderickx, G. J.; Van Geem K. M. and Marin G. B. (2017). Design and cold flow testting of a Gas-Solid Vortex Reactor demonstration unit for biomass fast pyrolysis, *Chemic- al Engineering Journal,* 329, 198–210. *http:// dx.doi.org/10.1016/j.cej.2017.06.003*

Jin, W.; Xiaoke, K. and Zhiwei, L. (2023). Three-Dimensional Simulation of the Pyrolysis of a Thermally Thick Biomass Particle. Energy & Fuels 2023, 37 (6), 4413- 4428. https:// doi.org/10.1021/acs.energyfuels.2c03 675

Jin, W. and Xiaoke, K. (2023). Numerical simulation of biomass steam gasification in an internally interconnected fluidized bed using a two-grid MP-PIC model. Chemical Engineering Science 2023, 272, 118608. https://doi.org/10.1016/j. ces.2023.118608

Johnson, P.; Nott, P. and Jackson, R. (1990). Frictional-collisional equations of motion for participate flows and their application to chutes, *Journal of fluid mechanics*, Retrieved from. *http:// journals.cambridge.org/abstract_S00 22112090001380*

Ku, X.; Li, T. and Terese, L. (2015). CFD–DEM simulation of biomass gasification with steam in a fluidized bed reactor, *Chemical Engineering Science*, 122, 270-283. http://dx.doi. org/10.1016/j.ces.2014.08.045

Liu, B.; Papadikis, K.; Gu, S.; Fidalgo, B.; Longhurst, P.; Li, Z. and Kolios, Z. (2017). CFD modelling of particle shrinkage in a fluidized bed for biomass fast pyrolysis with quadrature method of moment, *Fuel Processing Technology*, 164, 51–68. *http://dx.doi. org/10.1016/j.fuproc.2017.04.012*

Lun, C.K.K. (1984). Kinetic theories for granular flow: in-elastic particles in Couette Flow and slightly inelastic particles in a general flow field, *Journal of Fluid Mechanics*, 140 (1), 223–256. Retrieved from: http://

journals.cambridge.org/abstract_S0022112084000586

Moritiwon, O. J.; Afolabi, E. A;, Garba, M. U. and Aboje A. A. (2021). Experimental investigation of fast pyrolysis of Isoberlina doka-derived sawdust for bio-oil production, *Arabian Journal for Science and Engineering*, 1-11. *https://doi.org/10.1007/s13369-020-04960-2.*

Punsuwan N. and Tangsathitkulchai C. (2014). Product characterization and kinetics of bio-mass pyrolysis in a three-zone free-fall reactor, *International Journal of Chemical Engineering,* 1-10. *https://doi.org/10.1155/2014/986719*

Ramisetty, K. (2010). *Prediction of concentration profiles of a particle-laden slurry flow in horizontal and vertical pipes*, Oklahoma State University. *https://www.google.com/url?sa=t&source=web&rct=j&url=https://shareok.org/bitstream/handle/11244/10042/Ramisetty_okstate_0664M_11139.pdf%3Fsequence%3D1&ved=2ahUKEwiCzKvsnbTtAhVFJBoKHSeoDaYQFjAAegQIARAB&usg=AOvVaw0ykRi_vMOwbOIEByBudbqo*

Raval, A. (2008). *Numerical simulation of water waves using Navier-Stokes equations*, PhD thesis, University of leeds, White rose eThesis online, *Http://etheses.whiterose.ac.uk/11280/493287.pdf*

Runhui, Z.; Xiaoke, K.; Jianzhong, L. and Kun, L. (2023). Efficient Pyrolysis Model for Large Biomass Particles with Arbitrary Shapes Based on a Composed-Sphere Concept and Voronoi Tessellation. Energy & Fuels 2023, 37 (14), 10493-10505. https://doi.org/10.1021/acs.energyfuels.3c01269

Ruming, P.; Bachirou, G. L.; Yong, S.and Gérald, D. (2023). A multidimensional numeric study on smoldering-driven pyrolysis of waste polypropylene. Process Safety and Environmental Protection 2023, 172, 305-316. https://doi.org/10.1016/j.psep.2023.02.018

Shu, Z.; Wang, J.; Zhou, Q.; Fan, C. and Li, S. (2015). Evaluation of multifluid model for heat transfer behavior of binary gas-solid flow in a downer reactor, *Powder Technology*, 281, 34–48 (2015). *http://dx.doi.org/10.1016/j.powtec.2015.04.055*

Sambal, M.; Rogers, W. and O'Brien, T. (1993). MFIX documentation: Theory guide. … Note DOE/METC-95/1013 and …. Available at: *http://www.researchgate.net/profile/Madhava_Syamlal/publication/252563656_MFIXdocumentation_theoryguide/links/00b7d52fa5451d3321000000.pdf*

Versteeg, H. K. and Malalasekara, W. (2007). *An introduction to computational fluid dynamics- the finite volume method*, Pearson Prentice Hall, 2. *www.pearsoned.co.uk.*

Wang, A. and Chen, Q. (2012). A new empirical model for predicting single-sided, wind-driven natural ventilation in buildings, *Energy and Buildings*, 54, 386-394. *https://doi.org/10.1016/j.enbuild.2012.07.028.*

Yildiz, G.; Ronsse, F.; Duren, R. V. and Prins, W. (2016). Challenges in the design and operation of processes for catalytic fast pyrolysis of woody biomass, *Renewable and Sustainable Energy Review,*57, 1596–1610. *http://dx.doi.org/10.1016/j.rser.2015.12.202*

Yu, X.; Hassan, M.; Ocone, R. and Makkawi, Y. (2015). A CFD study of biomass pyrolysis in a reactor equipped with a novel gas–solid separator-II thermochemical performance and products*, Fuel Processing Technology*, 133, 51-63 *http://dx.doi.org/10.1016/j.fuproc.2015.01.002*